A Semi-local Surface Feature for Learning Successful Grasping Affordances

Mikkel Tang Thomsen, Dirk Kraft and Norbert Krüger
Maersk Mc-Kinney Moller Institute, University of Southern Denmark, Campusvej 55, 5230, Odense M, Denmark

Keywords: Computer Vision, Robotics, Grasp Affordance Learning.

Abstract: We address the problem of vision based grasp affordance learning and prediction on novel objects by proposing a new semi-local shape-based descriptor, the Sliced Pineapple Grid Feature (SPGF). The primary characteristic of the feature is the ability to encode semantically distinct surface structures, such as "walls", "edges" and "rims", that show particular potential as a primer for grasp affordance learning and prediction. When the SPGF feature is used in combination with a probabilistic grasp affordance learning approach, we are able to achieve grasp success-rates of up to 84% for a varied object set of three classes and up to 96% for class specific objects.

1 INTRODUCTION

An important problem that is being addressed in computer vision and robotics is the ability for agents to interact in previously unseen environments. This is a challenging problem as the sheer amount of potential actions and objects is infeasible to model. A way to overcome this infeasibility is to introduce and learn generic structures in terms of visual features and action representations to be reused over multiple actions and over different objects. It is well known that such reuseabliliy is occurring in the human brain, where the cognitive vision system have a generic feature representation with features of different sizes and level of abstractions that can be used as it fits, see (Krüger et al., 2013), also for a general overview of the human visual system from a computer-vision/machine learning perspective.

In this paper, we learn grasping affordances based on a novel semi-local shape-based descriptor named the Sliced Pineapple Grid Feature (SPGF). The descriptor is derived by k-means clustering (Lloyd, 2006) on radially organized surface patches with a defined centre surface patch (see Fig. 1b). The descriptor is able to represent both sides of a surface as well as non-existence of shape information. Both aspects are important when we want to code grasps as these are strong cues for potential grasp points.

By means of our descriptor and unsupervised learning, we are able to learn a discrete set of relevant semi-local descriptors that covers semantically distinct surface categories — which we call shape particles — such as "wall", "rim", "surface" (see Fig. 1h). In a second step, we associate grasp affordances to the shape particles by the probabilistic voting scheme in (Thomsen et al., 2015) which results in shape-grasp particles. These shape-grasp particles allow us to probabilistically code the success likelihood of grasps in relation to the shape particles (see Fig. 1i).

We evaluate our system on an object set covering three categories in a simulation environment. We show that we are able to reliable predict grasps with a success-rate of up to 96% for individual object classes and 84% for the full object set, when utilising two complimentary grasp types namely a narrow- and wide two finger pinch grasp.

The paper is organised as follows: In section 2, we relate our work to state-of-the-art in terms of feature- and model-based grasping of novel objects. Next in section 3, we introduce the SPGF shape descriptor and relate it to grasp affordances. We present the acquired results in section 5 both quantitatively and qualitatively based on the simulated experimental setup presented in section 4. In the conclusion, section 6, we discuss the results as well as future work.

2 RELATED WORK

Within vision based robotic grasping of unknown objects, two approaches are prevalent. First,

Thomsen, M., Kraft, D. and Krüger, N.
A Semi-local Surface Feature for Learning Successful Grasping Affordances.
DOI: 10.5220/0005784505620572
In *Proceedings of the 11th Joint Conference on Computer Vision, Imaging and Computer Graphics Theory and Applications (VISIGRAPP 2016) - Volume 3: VISAPP*, pages 564-574
ISBN: 978-989-758-175-5

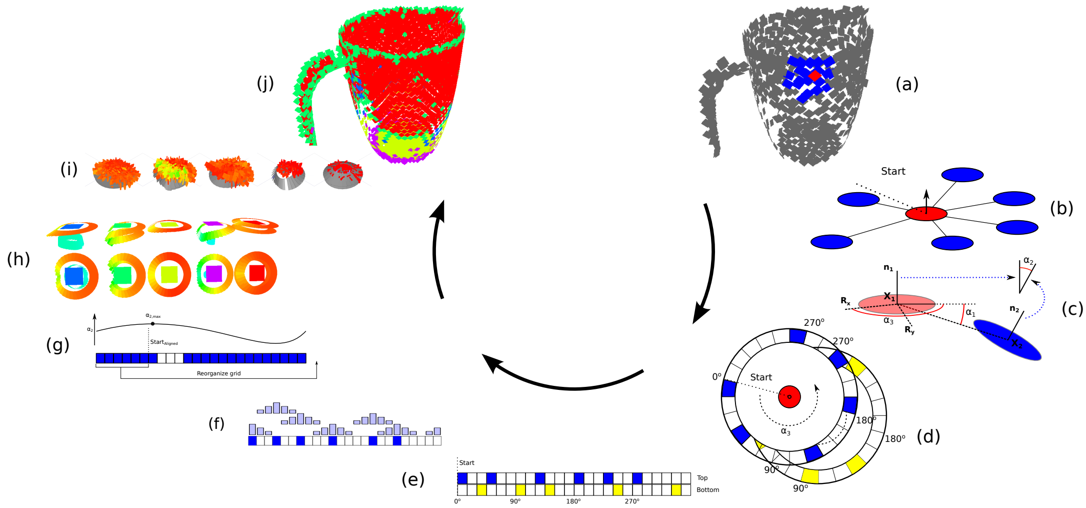

Figure 1: Overview of the feature creation and learning process for the SPGF feature. (a) A scene represented by τ features with a selected one (red) and its neighbours (blue) within a radius, r. (b) Selected feature and its neighbours. (c) Spatial relations between the central feature (red) and its neighbours. (d) Organization of the neighbours in two circular grid structures introduced in the plane of the central feature, one grid describing features with the normal in the same direction as the central one and one with normals pointing in the opposite direction of the central one. (e) Unfolding of the circular grids. (f) Performing a weighted moving average filter to fill up empty cells in the grids. (g) Alignment of the grids to the direction of highest curvature. (h) k-means clustering in the grid feature space resulting in a finite set of learned SPGF features. (i) Features with associated grasp affordances. (j) Inferred features on object.

model based approaches where the unknown object is approximated by simple shapes like bounding boxes (e.g. (Curtis et al., 2008)) or more advanced shapes like super-quadratics (e.g. (Huebner et al., 2008)). Other model based approaches are for example in (Detry et al., 2013) where object shapes are learned as prototypical parts that human demonstrated grasps are associated to. In work by (Kopicki et al., 2014) a combined contact- and hand-model based on visual appearance is learned for selecting successful grasp poses.

The other main branch in vision based grasping are feature based approaches, where visual features are either used as cues or in a combined way used as input for making grasp predictions. (Saxena et al., 2008) showed how features from 2D images could be used to find reliable grasp points for a dishwasher emptying scenario. In work by (Kootstra et al., 2012), it was shown how simple surface and edge features could be used for predicting grasps with a reasonable probability of success. In (Thomsen et al., 2015), visually triggered action affordances were learned by associating related pairs of small surface patches with successful grasping actions. Another feature-based approach is proposed in work by (Lenz et al., 2013). Here the visual feature representations were learned unsupervised using deep learning techniques as a preliminary step towards grasp learning. This work is of particular interest as it showed superior performance compared to a previous paper with fundamentally the same grasp learning approach but where the visual features were hand selected (Jiang et al., 2011). Other approaches that utilise deep learning techniques for unsupervised feature learning and later for grasp selection are work by (Redmon and Angelova, 2014) where AlexNet (Krizhevsky et al., 2012) has been adopted to use RGB-D data as input. In work by (Myers et al., 2015), Superpixel Hierarchical Matching Pursuit has been proposed and used to learn geometric visual features on RGB-D data on which tool affordance learning has been applied. For an extensive review of the work performed in the robotic grasping domain see (J. Bohg and Kragic, 2014).

In our work, we propose a novel semi-local shape descriptor, SPGF, aimed at grasp affordance learning. The SPGF feature allows for encoding of semantically rich local surface structures, including gaps and walls that can be found in multi-view or SLAM (Durrant-Whyte and Bailey, 2006) acquired scenes. When utilised for grasp affordance learning and prediction on previously unseen objects, the learned features demonstrates high performance. As the feature types are learned in an unsupervised way using k-means clustering, they are not strictly bound to the grasping actions and can therefore be utilised for different actions although this utility is only weakly exploited in this paper.

3 METHOD

The aim of the proposed SPGF feature is to provide a solid foundation for reliable grasp affordance learning and prediction. To achieve this, a number of desirable properties have been identified, that should be captured by the feature:

1. Encoding of local shape geometry in SE(3).
2. Encoding of double sided structures.
3. Encoding of gaps.
4. Rotation invariance.

An overview of the process is shown in Fig. 1, where the steps from object (Fig. 1a) to clustered reference features (Fig. 1h), denoted prototypes, to grasp association (Fig. 1i) can be followed. In the following subsections, first the feature creation process will be explained (Fig. 1a–g and section 3.1), next the learning process of extracting a small finite set of descriptive feature prototypes will be introduced (Fig. 1h and section 3.2). In section 3.3, the feature inference process, that allows for using the prototypes on novel situations will be addressed (Fig. 1j) and finally in section 3.4, the learned features are linked to grasping poses and grasp affordance learning (Fig. 1i).

As a starting point and input to the feature learning system, a set of scenes, represented by small surface patch descriptors (concretely texlets3D (Kraft et al., 2014)) are used, see Fig. 1a for an example. As a general notation the base features are described by a position $\mathbf{X}$ and a surface normal vector $\mathbf{n}$:

$$\tau = \{\mathbf{X}, \mathbf{n}\} = \{x, y, z, n_x, n_y, n_z\}, \quad |\mathbf{n}| = 1 \quad (1)$$

3.1 Feature Creation

We start out with a scene representation consisting of the above mentioned surfaces features (τ) and for each surface feature we follow the steps sketched below:

1. Find all the neighbours, within an Euclidean radius r, see Figs. 1a, 1b. This leads to a context-dependent number of neighbours (J).
2. For each of the J neighbours compute pairwise spatial relations between the centre feature (red) and the neighbour (blue). This will result in J pairwise relations, see Fig. 1c.
3. Split the neighbours into two sets based on the relation of their normals with respect to the centre feature; surface patches oriented in the same direction make up one set of relations (r_t), the others the second (r_b). Order the neighbours into two circular discretized grid structures based on the rotation around the normal of the centre feature, see Fig. 1d and Fig. 1e.

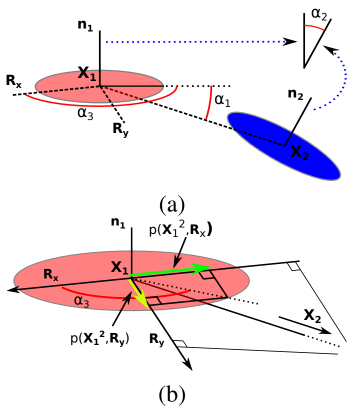

Figure 2: (a) The pairwise spatial relationships between the centre feature (feature one) and feature two utilised in this work. α_1 depict the angle between the plane of the centre feature (red) and the vector connecting the positions of the features ($\mathbf{X}_1^2$), α_2 depicts the angle between the surface normals of the two features, α_3 depicts the rotation angle around the normal of the centre feature ($\mathbf{n_1}$) from a reference direction, $\mathbf{R_x}$, on the plane to the projection of the connecting vector onto the plane. (b) A detailed view on how the angle α_3 is derived from the projection of the vector $\mathbf{X}_1^2$ onto the reference directions $\mathbf{R_x}$ and $\mathbf{R_y}$ (green and yellow arrows), from which α_3 can be derived.

4. Fill out empty grid locations by applying a weighted moving averaging filter over the grid structures to combat sampling artefacts, see Fig. 1f.
5. To achieve rotation invariance, the start point is moved simultaneously for the two grids to the grid-cell of highest curvature. In addition, the 6D pose of the centre feature is corrected to align one of the in plane axis with that direction, see Fig. 1g.
6. Finally, the top and bottom layer grids are concatenated into a feature vector, f, consisting of the aligned 6D pose of the centre surface feature and all the sorted relational values (r_t', r_b').

In the following subsections specific details are given for the spatial relationships (step 2, section 3.1.1) and the grid organizing (steps 3–6, section 3.1.2) procedures.

3.1.1 Spatial Relationship

The relational descriptor used in this work is based on a set of pairwise relations between surface patch features of the type described in Eq. 1. The pairwise relations resembles the ones proposed in (Wahl et al., 2003) and (Mustafa et al., 2013). The three different angular relations ($\alpha_1, \alpha_2, \alpha_3$) are visualised in Fig. 2 and described by Eqs. 2-4.

Before defining these angles a reference coordinate system ($\mathbf{R_x}$, $\mathbf{R_y}$, $\mathbf{n_1}$) for the centre patch needs to

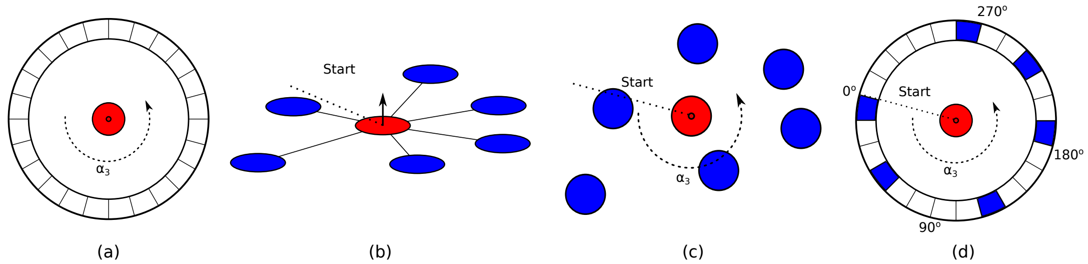

Figure 3: Introduction of the grid organization for a single layer ($\alpha_2 > 90°$ or $\alpha_2 < 90°$). (a) The proposed grid structure discretized into N_g cells. (b) An example with six neighbours with an arbitrary start direction. (c) Top view of the projection of the six neighbour positions in the plane of the red feature. (d) The six neighbours organised in the proposed discretized grid structure based on their angle around the normal of the red feature, α_3.

be defined. We choose the patch's normal ($\mathbf{n_1}$) as z-axis. $\mathbf{R_x}$ is chosen to be an arbitrarily direction in the plane of the first surface patch. The final axis ($\mathbf{R_y}$) can then be computed using the cross product of $\mathbf{n_1}$ and $\mathbf{R_x}$. Furthermore the vector connecting the two features ($\mathbf{X_1^2} = \mathbf{X_1} - \mathbf{X_2}$) and the projection of this vector on an axis ($p(\mathbf{X_1^2}, \mathbf{R_x}) = \frac{(\mathbf{R_x} \cdot \mathbf{X_1^2})}{||\mathbf{X_1^2}||}$) are needed to then define the angles between two features (τ_1, τ_2) as follows:

$$\alpha_1 = \frac{\pi}{2} - acos(\frac{\mathbf{X_1^2}}{||\mathbf{X_1^2}||} \cdot \mathbf{n_1}) \quad (2)$$

$$\alpha_2 = acos(\mathbf{n_1} \cdot \mathbf{n_2}) \quad (3)$$

$$\alpha_3 = atan2(p(\mathbf{X_1^2}, \mathbf{R_x}), p(\mathbf{X_1^2}, \mathbf{R_y})) \quad (4)$$

Together with the organisation in a grid structure, presented next, these measures are used to form the relational descriptor.

3.1.2 Organizing the Neighbourhood in a Sliced Pineapple Grid Structure

The next step is to organize the information about the neighbouring features into two circular grid structures. The two grid structures represent respectively a top layer (r_t) and a bottom layer (r_b). The top layer grid describes the neighbourhood of features with the normal in the same direction ($\alpha_2 < 90°$) as the centre feature and the bottom layer describes features with the normal in the opposite direction of the centre feature ($\alpha_2 > 90°$).

Both layers are then discretized into a circular grid, see Fig. 3(a), with a resolution of N_g. All neighbours are projected into the plane of the centre feature (see Fig. 3(c)) and their (α_1, α_2) are then placed into the rotational bin that corresponds to the specific α_3 value (see Fig. 3(d)). If multiple neighbours fall within the same cell, the average value of the relations are used. These steps are performed for both, the top layer and the bottom layer, resulting in two circular grids representing the neighbourhood of a feature. The grids are then unfolded to two flat grids.

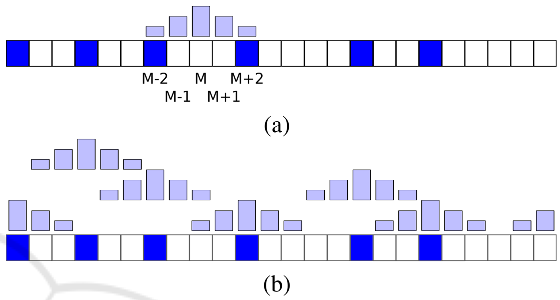

Figure 4: Weighted moving average of the grid structure. (a) Illustrates how the cell at M is equally contributed to by the cell at M+2 and M-2, practically resulting in the average of the two. (b) A practical illustration of how the cells with datapoints (coloured ones) affect the surrounding cells with the weight depicted by the size of the bars.

Weighted Moving Average. Depending on the number of neighbours within the radius, r, and the discretization of the grid, the grid structures will consist of a substantial amount of cells where no data is found. These undefined cells are considered to be of two types.

1. They are a result of the general low density of the underlying feature representation within a small radius.
2. They are real gaps depicting a direction where no visual data exist.

The second type is of specific interest, as gaps can be a strong visual cue (e.g., for affording pinch grasps or indicating open structures), whereas the first type is to be avoided. To address this artefact of sampling, a weighted moving average (WMA) is performed on the feature vectors to fill gaps. In addition, the WMA improves the robustness of the feature representation.

In Fig. 4, the principle is illustrated by showing the contribution that the existing datapoints give to neighbouring cells in the grid, hereby filling out small gaps in the representation. The WMA for the cells is performed for the two relations (α_1, α_2) independently. It should be noted, that if no value exists in a cell, it will not contribute to the average. The length of the filter n, determines the amount of smoothing.

After the moving average operation, gaps can still exist depending on the length of the averaging filter. These gaps are considered to be the "real" gaps. To encode the real gaps in a meaningful way that can be handled by the vector based k-means clustering, they are described with saturated values of the parameters. For α_1 this means $-90°$ and for α_2 this means $90°$ and $180°$ for the top and bottom grid respectively.

Alignment of Grid. As a final step, the feature grid is aligned to make the representation rotation invariant. The selected alignment is at the place of highest curvature on the top part of the feature vector. This equals finding the grid cell with the largest value of α_2 and reorganising the grid such that this cell becomes starting point, see Fig. 5 and also Fig. 10, where the alignment of the learned features are presented.

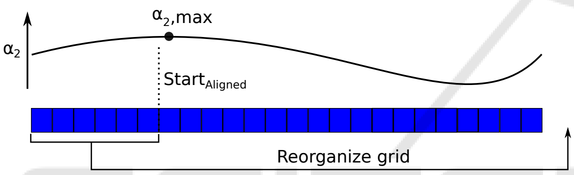

Figure 5: Alignment of the feature grid starting point based on the maximum value of α_2, $\alpha_{2,max}$, of the top layer grid. The variation of α_2 over the grid is visualised above the grid. Both top layer and bottom layer are aligned to this new starting point and the grids are reorganized accordingly.

Based on the aligned starting point, a 6D pose is computed (update the reference direction $\mathbf{R_x}$ and $\mathbf{R_y}$, see subsection 3.1.1) to place the feature with respect to the world. Finally, the aligned top (r_t') and bottom (r_b') grids are concatenated into a combined feature vector f and the aligned 6D pose of the centre feature is added.

3.2 Feature Learning

Once this representation is designed, we are interested in finding reference features, called prototypes, that are able to describe the features present in the training object scenes in the best way. For that the following two steps are taken.

1. Perform the feature creation steps, see section 3.1, for the full object set, resulting in a large set of feature vectors, $f_i : i = 1, ..., L$
2. Perform a k-means Euclidean clustering (Lloyd, 2006) in the relational space of the f's (only the r_t', r_b' parts, not the position or orientation of the centre). K defines the number of prototypes (P_{id}) that the learned dictionary, ($\mathbb{P}$) Eq. 6, should consist of. The prototypes are described by a point in the relational-vector space, see Eq. 5 and Fig. 1h.

$$\begin{aligned} P_{id} &= \{\alpha^0_{1,id}, \alpha^0_{2,id}, \alpha^1_{1,id}, \alpha^1_{2,id}, ..., \\ &\quad \alpha^{2N_g-1}_{1,id}, \alpha^{2N_g-1}_{2,id}\} \in \mathbb{R}^{2\cdot 2N_g} \qquad (5)\\ \mathbb{P} &= \{P_1, P_2, ..., P_K\} \qquad (6) \end{aligned}$$

3.3 Feature Inference

Provided a set of feature prototypes has been learned, the inference process of utilising them to describe novel objects is introduced with the following steps:

1. Perform the feature creation process, see section 3.1, for an object where features are to be inferred. This results in a set of feature vectors $\mathbb{F}$.
2. For every $f \in \mathbb{F}$, find the closest prototypes P_{id} in the set of learned prototypes $\mathbb{P}$ using the Euclidean distance on the relation part (only r_t', r_b') of f, see Eq. 7. Given this id, a new feature T is created that consists of the feature pose (position $\mathbf{X}$ and quaternion $\mathbf{q}$,given by f) and the computed id. See also Fig. 1j for an example object with inferred features.

$$D(f, P_{id}) = \sqrt{\sum_{i=0}^{2N_g-1} (\alpha^i_{1,f} - \alpha^i_{1,id})^2 + (\alpha^i_{2,f} - \alpha^i_{2,id})^2} \qquad (7)$$

$$\begin{aligned} id &= \underset{id}{\operatorname{argmin}}(D(f, P_{id}) : P_{id} \in \mathbb{P}) \qquad (8)\\ T &= \{\mathbf{X}, \mathbf{q}, id\} \qquad (9) \end{aligned}$$

3.4 Grasp Affordance Learning

In order to utilize the learned SPGF features for grasp affordance learning (Fig. 1i), the pose of the visual feature is linked to the pose of a grasp by a 6D pose transformation, see Fig. 6. We use the method introduced by (Thomsen et al., 2015) to do this. In the following, we give a brief overview of the method for details please see (Thomsen et al., 2015).

The shape-grasp space is occupied by a large set of shape-grasp particles describing how individual actions relate to individual features. To condense the information for reliable action predictions, a neighbourhood analysis is performed to compute the success probability of a given point in the space as well as the amount of similar points (called support). Next, the learned shape-grasp particle space is condensed to only consist of points that have a significant support. This knowledge is then used to vote for grasps in novel situations with the probability associated during learning. This results in a set of grasps, that can be ranked based on the predicted success probability and the amount of votes.

4 EXPERIMENTS

The experiments performed in this work are based on a simulated set-up created in RobWorkSim (Jørgensen et al., 2010), see Fig. 7. The set-up consists of simulated RGB-D sensors and the object of interest in the centre, from which a visual object representation is acquired, see Fig. 7a and Fig. 1a for an extracted scene. It should be noted that modelled sensor noise is added and that the four views still lead to incomplete models that the four views introduce. In addition to the scene rendering, the simulation environment is also utilised for performing grasping simulations by means of the simulation framework RobWorkSim. The simulator is based on a dynamics engine that simulates object dynamics in terms of the contact forces that emerge during a grasping execu-

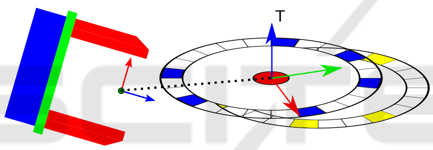

Figure 6: Linking of a grasping action and a visual feature, T, described by the 6D pose transformation, a grasp outcome (success/failure) and an id (relating to the corresponding P_{id}).

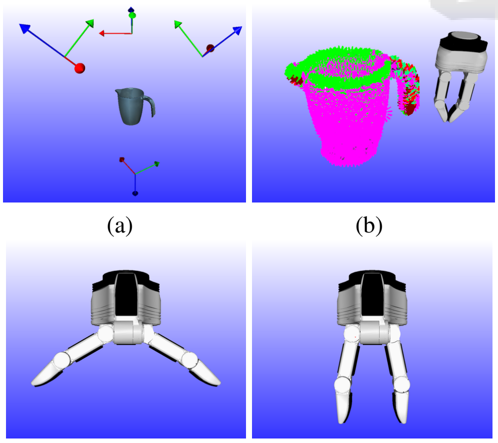

(a) (b) (c) (d)

Figure 7: Experimental setup. (a) Visualisation of the simulated sensor set-up. Four RGB-D sensors, represented by the four frames, surround the object. (b) Outcome of grasp simulations performed in RobWorkSim (Jørgensen et al., 2010) with the NPG (Narrow Pinch Grasp), see (d). Red and pink equals failed grasps and green depicts successful grasps. (c) The Wide Pinch Grasp (WPG).

Figure 8: A subset of the 50 objects used in the experimental work. The 3D models have been taken from the KIT database (Kasper et al., 2012) and from archive3d (Archive3D,). See (Thomsen et al., 2015) for the full object set.

tion. Grasping is performed with a simulated version of the Schunk SDH-2 hand with two different grasp preshapes, a wide pinch grasp (WPG) and a narrow pinch grasp (NPG), see Figs. 7(c) and 7(d). The experiments are performed on an object set consisting of 50 objects, see Fig. 8 for a subset. The object are classified into three classes, containers, boxes and curved objects.

Evaluation Score. A 5-fold cross-validation is performed to evaluate the learned prototypes for prediction of grasps on novel objects. The learning and evaluation of features and grasps are performed on the full object set. However, in order to compare the achieved results with work of (Thomsen et al., 2015) on the same dataset the object class-wise grasp prediction performance is also presented.

To measure the performance of our method, we use the success-rate of the highest ranked grasps from the votes of shape-grasp particles. The N highest ranked grasps (in a combined selection of support and probability, here the support depict that a grasp have achieved a significant amount of votes) are compared to the actual outcome of the grasps and the success-rate is computed as follows:

$$\text{success-rate} = \frac{N_{success}}{N} \tag{10}$$

Feature Learning Parameters. For the feature learning part five parameters need to be set. A radius, r, of 0.03m is used. The discretization of the circular grid, N_g, is set to 36, equalling slices of 10°. The WMA filter is set to be of length 6 resulting in an average over 60° in each direction. Finally, the amount of clusters, (K learned features), are varied between 5 and 25 as a part of the experimental results. In the presented results N=10 is used.

.

Table 1: Success-rate for Narrow Pinch Grasp (NPG), Wide Pinch Grasp (WPG) and Combined Grasp (CG). Results are based on the average success-rate of the 10 highest predicted grasps for each object. Random depict the chance for randomly selecting a successful grasp in the set. [*] depict the results achieved in (Thomsen et al., 2015).

		Containers [%]			Boxes [%]			Curved [%]			All [%]		
		NPG	WPG	CG	NPG	WPG	CG	NPG	WPG	CG	NPG	WPG	CG
K	5	48.0	26.5	30.5	12.9	80.0	80.0	6.3	93.8	93.8	24.8	63.0	64.6
	10	85.0	46.5	59.5	13.6	84.3	84.3	6.3	95.0	95.0	39.8	72.6	77.8
	15	82.0	34.0	63.0	14.3	77.1	77.1	6.3	88.1	88.1	38.8	63.4	75.0
	20	78.0	40.5	74.0	13.6	87.9	87.9	6.3	92.5	92.5	37.0	70.4	83.8
	25	79.0	33.5	71.5	12.9	85.7	85.7	6.3	95.6	95.6	37.2	68.0	83.2
[*]		68	-	-	-	84	-	-	84	-	-	-	-
random		10.6	11.5	-	4.8	46.6	-	4.4	51.3	-	7.0	34.1	-

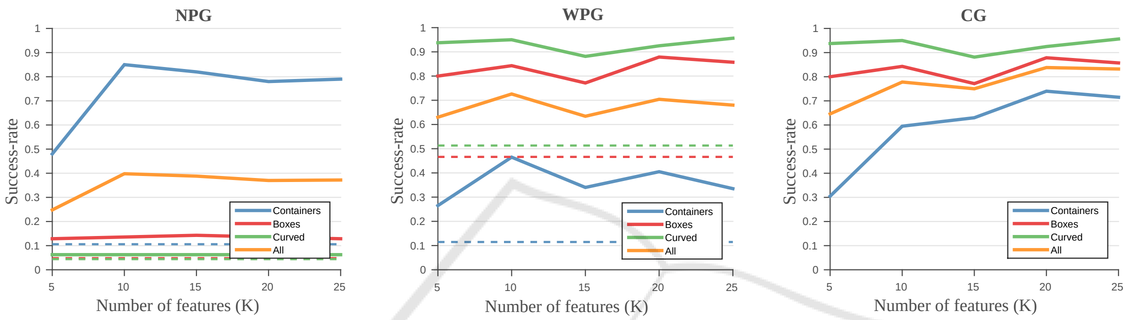

Figure 9: The results for the grasp predictions for the different object classes as well as for all the objects, presented for the two different grasp types NPG and WPG and for the combined grasp CG. The dashed lines depict the random chance of selecting a successful grasp for the individual object classes.

5 RESULTS

First, an evaluation of the grasp prediction performance is presented for different amounts of learned features (different K's) (section 5.1). Secondly, a qualitative assessment of a set of learned features and learned associated grasps is presented (section 5.2).

5.1 Grasp Prediction Evaluation

In Tab. 1 and Fig. 9, the results are presented for the individual object classes for the two different grasp types (NPG, WPG) (see Fig. 7) as well as for the grasp performance when the highest ranked of the two grasp types are chosen (CG). These measures are also presented for the full object set. All the results are presented for five different values of K. The table also shows the performance in (Thomsen et al., 2015) and the chance for a random selected grasp to be successful.

For the container objects, the performance of the NPG grasp is generally high around 80% for K larger than five, whereas the performance with WPG grasp is in the range of 27% – 47%. When the best of the two grasp types is chosen, CG, the performance is in the range of 60% – 74% for K larger than five. The scores should be compared with the random chance of selecting one of the two grasps (11%). For the box objects, the NPG grasp have a success-rate in the region of 10% – 15% whereas the WPG grasp performs with a success-rate in the range of 77% – 88%. Similar results as the WPG is achieved for the CG grasp. For the curved objects, the NPG grasp have a success-rate of 6% and the WPG grasp performs in the range of 88% – 95%. The CG grasp performs similar to the WPG grasp. For all the objects, the NPG grasp performance is in the range of 25% – 40% whereas the WPG performs in the range of 63% – 73%. When combined, the performance goes up to be in the range of 65% – 84%.

When comparing the scores for the individual grasp types, NPG and WPG, with the performance of the CG, we see, that for the container objects the CG score (31% – 74%) is performing worse than the NPG (48% – 85%) and the WPG (27% – 41%) whereas for the Box and Curved objects the CG performance (77% – 87% and 88% – 96%) is comparable to the score of the highest of the individual grasp types (88% and 95%). This difference is explained by the fact that the random chance of selecting a successful WPG

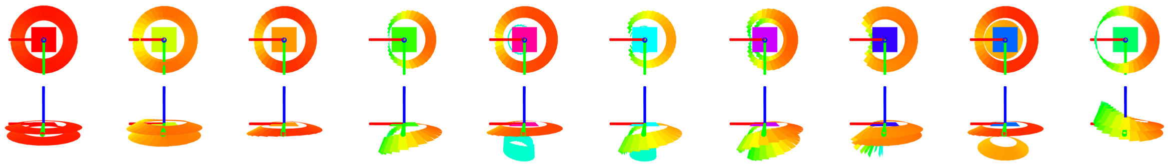

Figure 10: Visualisation of a learned set of visual features with K=10. The features are denoted 1 to 10 from left to right. The bottom and top rows show the same features from different angles. In addition to the actual inclination of the outer ring feature, the colour also denote the angle difference to the normal of the centre feature, green/cyan depict strong curvature whereas red depict none or little curvature. The orientation of the features are described by the inlaid frames (red, green and blue sticks). The colour in the centre of the features is used for encoding the inferred features on the novel objects, see Fig. 11.

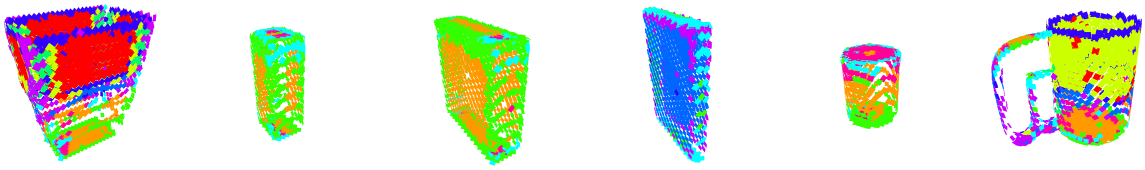

Figure 11: Example objects with inferred learned features. See the features in Fig. 10 and the corresponding colour coding to interpret the objects.

grasp is significantly higher than the chance for randomly selecting a NPG grasp. For the container object set it means that the grasp votes from the WPG learned affordances tend to dominate the NPG learned affordances, resulting in the lower combined score.

When comparing the results with the achieved scores in (Thomsen et al., 2015), superior performance is achieved, despite the fact that the conditions for the results acquired in this work is significantly more difficult due to that visual and action training is performed on the full object set as compared to the class-wise approach in (Thomsen et al., 2015). The performance on the individual object classes for the NPG and WPG perform better than the results acquired in (Thomsen et al., 2015) for the largest amount of Ks and in particular for K larger than five. The CG performance for the different classes also performs better than the individual grasps from (Thomsen et al., 2015) for a specific K. For K=20, the CG container score (74%) outperforms the NPG score (68%) from (Thomsen et al., 2015). For the boxes, the CG score (87%) outperforms the WGP score (84%) from (Thomsen et al., 2015) and for the curved objects, the CG score (93%) outperforms the WPG score (84%) from (Thomsen et al., 2015). Finally, the achieved score of 84% probability for selecting a successful grasp, CG, for the full object set is comparable to the highest achieved score for the individually grasp types in (Thomsen et al., 2015) for K=20.

5.2 Qualitative Assessment

In Fig. 10, the learned features from one of the folds are visualised for K=10. In Fig. 11, a subset of the novel objects in the same fold is shown with inferred features. The second figure can be useful to understand what the features describe. Multiple meaningful structures can be identified when assessing the features qualitatively, see Fig. 10. There are wall features with different curvature (1 and 2). Walls at an edge (7). Wall that have a gap which is identified as a rim (8). A surface feature with slight curvature (3) and surface edge structures (4, 5 and 6) with a varying degree of curvature.

In Figs. 12 and 13, the learned visual features are shown with the associated learned grasp affordances, in terms of coloured stick figures that depict the orientation of the grasps with respect to the feature. When assessing the features from the NPG (Fig. 12), only feature eight seems to be a reliable predictor for successful grasps. This feature describes the rim of a wall which explains the good performance as it intuitively is a good place to try a narrow pinch grasp. Some of the other features show some performance potential, for instance feature one, that describes a wall structure. A wall is intuitively graspable by a NPG grasp, but because it is found in a uniform area, one DOF in the pose is ill defined resulting in a low but rather uniform success probability around this DOF.

For the case of the WPG grasp, visualised in Fig. 13, the results are quite different. For the mostly flat structures (1 and 3), areas of high probability are not found. However for the highly curved features that somehow relate to edges (2, 4, 6 and 10) there are structures that suggest very high likelihood of grasp success. For features (2, 4 and 10) high probability areas are found in a somehow box structure aligned to the feature and below the features (the third column shows the bottom view). For feature six, the high probability areas are also found towards the normal

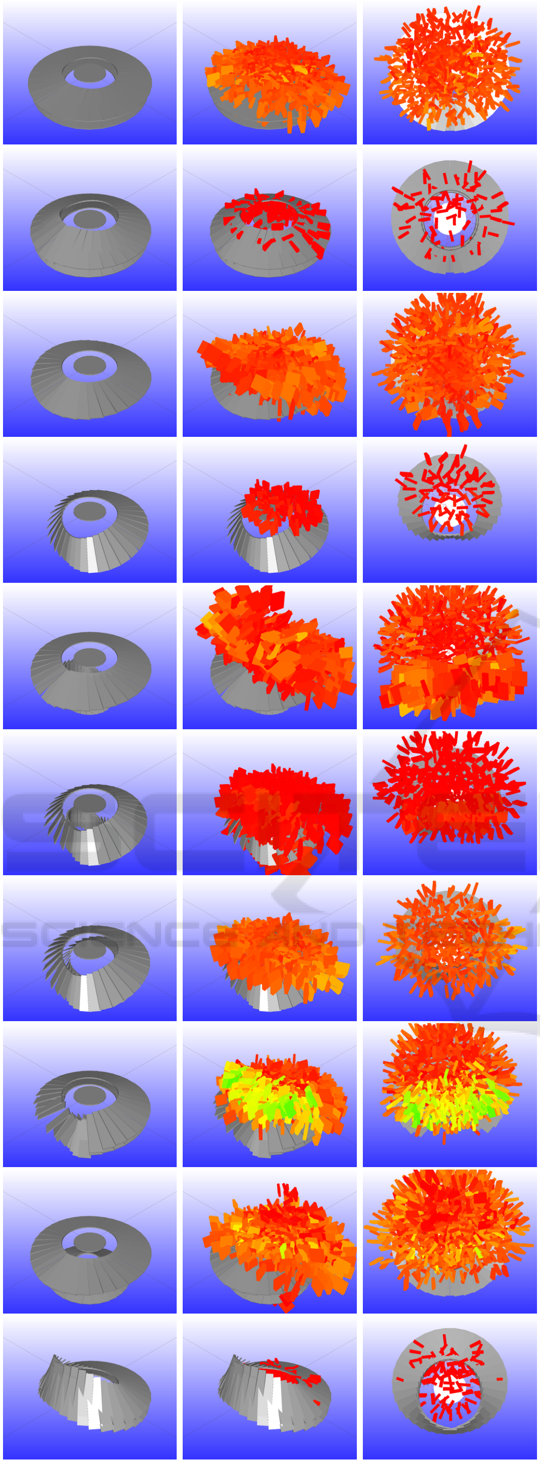

Figure 12: Visualisation of the visual features with the learned grasp affordances for the NPG grasp. The features are denoted 1 to 10 from top to bottom. Red depict low probability (0.0) of success. The colour changes towards green that depict a success probability of 1.0. First column show the features, the second column show the features with associated grasp from a perspective view and the third column show the features from a top view.

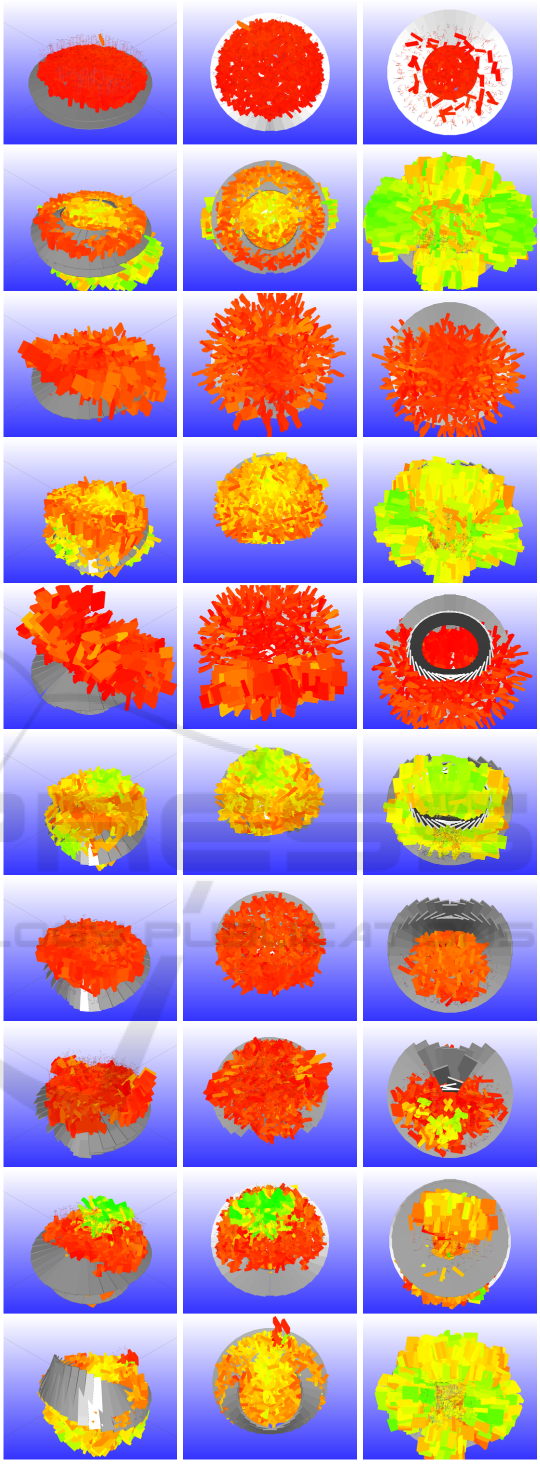

Figure 13: Visualisation of the visual features with the learned grasp affordances for the WPG grasp. The features are denoted 1 to 10 from top to bottom. Red depict low probability (0.0) of success. The colour changes towards green that depict a success probability of 1.0. First column shows the features from a perspective view. The second column, from a top view and the third column, from a bottom view. See also the first column of Fig. 12 for a view of the features without grasps.

of the centre feature. When this is matched with the inferred features on the fourth object in Fig. 11, this seems reasonable.

Finally, the qualitative result show that a diverse set of features are needed for predicting even slightly different actions with high rates of success. Exemplified by the fact that only a single prototype is good for the NPG grasp whereas others are suitable for the WPG grasp. This is an indication that our unsupervised approach for prototype learning based on the occurrence in the object set is a reasonable way to go.

6 CONCLUSION

In this paper, we have proposed, the Sliced Pineapple Grid Feature (SPGF), a novel semi-local shape-based descriptor, with the aim of utilising it for grasp affordance learning. The descriptor has a number of key properties such as its ability to encode double sided structures, encoding of gaps as well as being rotational invariant. As the extraction of a specific discrete set of shape descriptors is based on an unsupervised approach, the amount of features can be tuned for different applications or object sets. When utilising the learned features for grasp affordance learning and afterwards use the learned knowledge on novel situations, our system is able to predict grasp success with a rate of up to 96% for individual object classes and up to 84% when applied to an object set consisting of three classes of objects.

By utilising the learned features, the performance is better or comparable to the best results achieved in (Thomsen et al., 2015) performed on the same dataset despite that the learning conditions in this work are significantly more difficult. Regardless of the respectable performance of the grasp affordance system when applied to the full object set, the potential of the system is not yet fully realized, primarily illustrated by the fact that the CG performance for the container objects is well below the highest achieved score for the individual grasp types WPG and NPG. The primary reason for this is an unbalanced dataset, as the chance of randomly selecting a successful WPG grasp is significantly higher than the chance of randomly selecting a NPG grasp. This means that the votes from WPG tend to dominate the votes from NPG, resulting in a worse combined score.

From a qualitative perspective, the learned features exhibit similarity to structures that can be identified as building blocks of objects such as "walls", "rims", "edges", "surfaces" and others. Furthermore, the results indicate that different features are suitable for different affordances, in our work demonstrated by the two grasp types. Given the intuitiveness of the learned surface structure, a natural next step is to combine these into more elaborated features.

ACKNOWLEDGEMENT

The research leading to these results has received funding from the European Community's Seventh Framework Programme FP7/2007-2013 (Specific Programme Cooperation, Theme 3, Information and Communication Technologies) under grant agreement no. 270273, Xperience.

REFERENCES

Archive3D. Archive3d free online cad model database. http://www.archive3d.net.

Curtis, N., Xiao, J., and Member, S. (2008). Efficient and effective grasping of novel objects through learning and adapting a knowledge base. In *IEEE International Conference on Robotics and Automation (ICRA)*, pages 2252–2257.

Detry, R., Ek, C. H., Madry, M., and Kragic, D. (2013). Learning a dictionary of prototypical grasp-predicting parts from grasping experience. In *IEEE International Conference on Robotics and Automation*.

Durrant-Whyte, H. and Bailey, T. (2006). Simultaneous localization and mapping: part i. *Robotics Automation Magazine, IEEE*, 13(2):99–110.

Huebner, K., Ruthotto, S., and Kragic, D. (2008). Minimum volume bounding box decomposition for shape approximation in robot grasping. In *Robotics and Automation, 2008. ICRA 2008. IEEE International Conference on*, pages 1628–1633. IEEE.

J. Bohg, A. Morales, T. A. and Kragic, D. (2014). Data-driven grasp synthesis a survey. *IEEE Transactions on Robotics*, 30(2):289–309.

Jiang, Y., Moseson, S., and Saxena, A. (2011). Efficient grasping from rgbd images: Learning using a new rectangle representation. In *ICRA'11*, pages 3304–3311.

Jørgensen, J. A., Ellekilde, L.-P., and Petersen, H. G. (2010). RobWorkSim - an Open Simulator for Sensor based Grasping. *Robotics (ISR), 2010 41st International Symposium on and 2010 6th German Conference on Robotics (ROBOTIK)*, pages 1 –8.

Kasper, A., Xue, Z., and Dillmann, R. (2012). The KIT object models database: An object model database for object recognition, localization and manipulation in service robotics. *The International Journal of Robotics Research*.

Kootstra, G., Popović, M., Jørgensen, J. A., Kuklinski, K., Miatliuk, K., Kragic, D., and Krüger, N. (2012). Enabling grasping of unknown objects through a synergistic use of edge and surface information. *Has been accepted for Internation Journal of Robotic Research.*

Kopicki, M., Detry, R., Schmidt, F., Borst, C., Stolkin, R., and Wyatt, J. L. (2014). Learning dexterous grasps that generalise to novel objects by combining hand and contact models. In *to appear in IEEE International Conference on Robotics and Automation*.

Kraft, D., Mustafa, W., Popovic, M., Jessen, J. B., Buch, A. G., Savarimuthu, T. R., Pugeault, N., and Krüger, N. (2014). Using surfaces and surface relations in an early cognitive vision system. *Computer Vision and Image Understanding*.

Krizhevsky, A., Sutskever, I., and Hinton, G. E. (2012). Imagenet classification with deep convolutional neural networks. In *Advances in neural information processing systems*, pages 1097–1105.

Krüger, N., Janssen, P., Kalkan, S., Lappe, M., Leonardis, A., Piater, J., , Rodríguez-Sánchez, A. J., and Wiskott, L. (2013). Deep hierarchies in the primate visual cortex: What can we learn for computer vision? *IEEE PAMI*, 35(8):1847–1871.

Lenz, I., Lee, H., and Saxena, A. (2013). Deep learning for detecting robotic grasps. *CoRR*, pages –1–1.

Lloyd, S. (2006). Least squares quantization in pcm. *IEEE Trans. Inf. Theor.*, 28(2):129–137.

Mustafa, W., Pugeault, N., and Krüger, N. (2013). Multi-view object recognition using view-point invariant shape relations and appearance information. In *IEEE International Conference on Robotics and Automation (ICRA)*.

Myers, A., Teo, C. L., Fermüller, C., and Aloimonos, Y. (2015). Affordance detection of tool parts from geometric features. In *ICRA*.

Redmon, J. and Angelova, A. (2014). Real-time grasp detection using convolutional neural networks. *CoRR*, abs/1412.3128.

Saxena, A., Driemeyer, J., and Ng, A. Y. (2008). Robotic grasping of novel objects using vision. *Int. J. Rob. Res.*, 27:157–173.

Thomsen, M., Kraft, D., and Krüger, N. (2015). Identifying relevant feature-action associations for grasping unmodelled objects. *Paladyn, Journal of Behavioral Robotics*.

Wahl, E., Hillenbrand, U., and Hirzinger, G. (2003). Surflet-pair-relation histograms: a statistical 3d-shape representation for rapid classification. In *3-D Digital Imaging and Modeling, 2003. 3DIM 2003. Proceedings. Fourth International Conference on*, pages 474–481. IEEE.